Functionalization of graphene quantum dots by fluorine: Preparation, properties, application, and their mechanisms

Cite as: Appl. Phys. Lett. **110**, 221901 (2017); https://doi.org/10.1063/1.4984238
Submitted: 02 March 2017 . Accepted: 15 May 2017 . Published Online: 30 May 2017

Wenbin Zuo, Libin Tang, Jinzhong Xiang, Rongbin Ji, Lin Luo, Lukas Rogée, and Shu Ping Lau

Functionalization of graphene quantum dots by fluorine: Preparation, properties, application, and their mechanisms

Wenbin Zuo,[1] Libin Tang,[2,a)] Jinzhong Xiang,[1,b)] Rongbin Ji,[2,c)] Lin Luo,[2] Lukas Rogée,[3] and Shu Ping Lau[3]
[1]*School of Materials Science and Engineering, Yunnan University, Kunming 650091, People's Republic of China*
[2]*Kunming Institute of Physics, Kunming 650223, People's Republic of China*
[3]*Department of Applied Physics, The Hong Kong Polytechnic University, Hung Hom Kowloon, Hong Kong*

(Received 2 March 2017; accepted 15 May 2017; published online 30 May 2017)

Graphene quantum dots (GQDs) possess unique photoelectronic properties ascribed to quantum confinement and edge effects, which have evoked important development and wide application in the optoelectronic field. Doping GQDs with heteroatoms can further modulate the energy band structure and thus produce unexpected properties. Herein, we obtained fluorine-doped GQDs (F-GQDs) by adopting an effective preparation technique, which includes the treatment of the as-prepared reaction precursor, fluorinated carbon fibers, with ultrasonic liquid phase exfoliation. The proposed method is simple, handy, and low-cost, opening up an alternate approach to prepare F-GQDs. Through multiple characterization techniques, the effective incorporation of fluorine in GQDs was confirmed, and the as-prepared F-GQDs exhibit excellent photoelectrical properties and good ultraviolet absorption performances. Accordingly, we have fabricated a vertical photovoltaic UV detector based on F-GQDs. The unoptimized device has an exceptionally large ratio of photocurrent to dark current of magnitude $\sim 10^5$, and its detectivity (D^*) could stabilize at around 10^{12} Jones at room temperature under $\lambda = 365$ nm light irradiation and reverse bias voltage. *Published by AIP Publishing.* [http://dx.doi.org/10.1063/1.4984238]

As a newly emerging zero-dimensional (0D) carbon nanomaterial, graphene quantum dots (GQDs) present a series of outstanding optical and electrical properties due to their special qualities such as strong photoluminescence (PL), excellent biocompatibility, hypotoxicity, water solubility, and a tunable bandgap.[1–5] As we know, the exceptional properties of GQDs have expanded the application of traditional zero-bandgap 2D graphene to include optoelectronic devices, ascribed to the quantum confinement and edge effects. Because of that, GQDs have aroused extensive interest and study among scientific researchers. Up till now, GQDs were developed rapidly for solar cells,[6] photodetectors,[7] bioimaging,[8] and light emitting diodes.[9] In order to extend the application of GQDs further, doping with heteroatoms is an effective way for material modification. By doping, one can effectively engineer the tunable gap in GQDs, modify the surface structure, and add other functional groups to realize chemical functionalization.[10,11] Kundu and co-workers have developed a rapid and easy technique to synthesize N, F, and S co-doped GQDs with customized ionic liquid by microwave treatment, and thus improved the photoluminescence quantum yield (PLQY) (70%) of GQDs. Meanwhile, N, F, and S co-doped GQDs may induce defect clusters and lack of practical applications.[12] After doping with heteroatoms, the properties of GQDs have changed significantly; it is expected to further promote the development and application of doped GQDs in relevant fields.

Graphene-based materials exhibit high stability, special carrier transport properties, unique optical response, and preferable PL properties by introducing fluorine element.[13–17] In this letter, we report a facile method to prepare fluorine doped GQDs (F-GQDs), using cheap and commonly available degreasing cotton as the carbon source, followed by hydrothermal synthesis reaction to achieve the precursor fluorinated carbon fibers (F-CFs), which finally undergo ultrasonic liquid phase exfoliation to obtain F-GQDs. Meanwhile, the as-prepared F-GQDs have been characterized by their morphological structure, elementary composition, and photoelectric properties. Compared with the other method,[18] this approach is simple and handy without the need of Fluorinated graphene (FG) as precursor, which greatly reduces the cost of raw materials. We have fabricated a vertical UV photodetector based on F-GQDs to study the application in optoelectronics, in which the F-GQDs are used as a light sensitive and absorbing layer. We made a preliminary exploration on the application of F-GQDs in the field of photoelectric detection and found that the unoptimized device had an exceptionally large photocurrent to dark current ratio of magnitude $\sim 10^5$, and the detectivity (D^*) stabilized at around 10^{12} Jones under $\lambda = 365$ nm light irradiation.

The chemical reagents used in the experiments were obtained by commercial means and used without further purification.

F-GQDs were prepared by a method with hydrothermal assistance and ultrasonic liquid phase exfoliation. 5 g of degreasing cotton was used as the carbon source and annealed at 1000 °C for 1 h until it was fully carbonized into carbon fibers (CFs), followed by grinding these CFs into black powder. Next, 1 g of CFs was transferred to a Teflon container together with 15 ml of HF and 24 ml of DI-water. The mixture was led to react hydrothermally at 170 °C for 8 h under

a)E-mail: scitang@163.com
b)E-mail: jzhxiang@ynu.edu.cn
c)E-mail: jirongbin@gmail.com

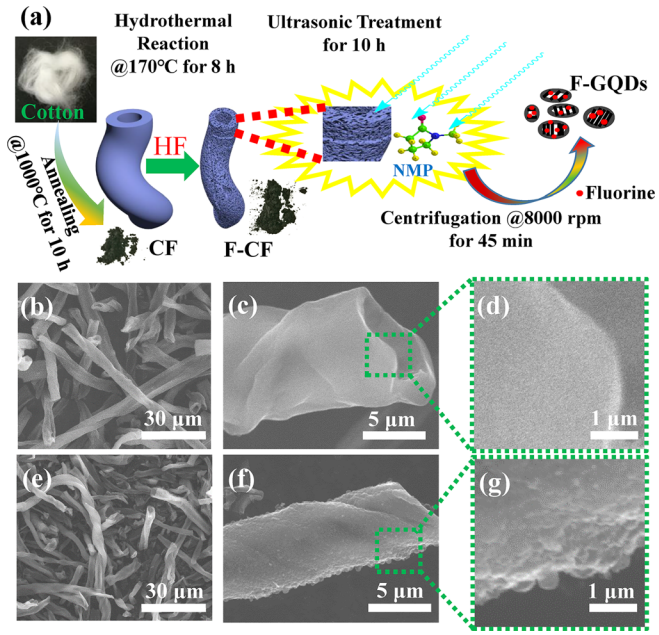

FIG. 1. (a) The illustration of relevant intermediates and treating processes to obtain F-GQDs. (b) and (e) The SEM images of holistic CFs and F-CFs. (c) and (f) The SEM images of CF and F-CF. (d) and (g) The surface morphology and edge structure of CF and F-CF, respectively.

ambient pressure, then led to cool down to room temperature, and finally washed with DI-water until its pH level was close to neutral. The residue was collected and dried at 80 °C for 30 min to prepare reaction precursor F-CFs. 0.5 g of F-CFs was dispersed into 80 ml *N*-methylpyrrolidone (NMP) and then subjected to ultrasonic treatment for 10 h with a frequency of 53 kHz until the solution turned black. The solution was centrifuged at 8000 rpm for 45 min. After centrifugation, the resulting grey colored upper part of the solution, which is the desired F-GQDs solution, was collected via a pipette, and the F-GQDs powder was obtained after evaporating that solvent. As reference, GQDs were obtained from CFs by ultrasonic liquid phase exfoliation in the same way as the F-GQDs.

Figure 1(a) illustrates the formation of CFs from the carbon source degreasing cotton by annealing, then the fluorination reaction of CFs with HF to form F-CFs, and the follow-up procedure to obtain F-GQDs via ultrasonic liquid phase exfoliate F-CFs. Both sp^2 and sp^3 carbon atoms exist in CFs. The scanning electron microscopy (SEM) images of holistic CFs and F-CFs are shown in Figs. 1(b) and 1(e), respectively. They are showing tubular and staggered overlapping distributions with less than 10 μm in diameter. Through the comparison between a single CF and F-CF SEM image, shown in Figs. 1(c) and 1(f), we found that the F-CF was slimmer than CF, and the surface of F-CF became rough due to corrosion by the F atoms[19] after CF reacted with HF under hydrothermal synthesis conditions, that is, at high temperature and high pressure. In the corresponding areas highlighted in green, the surface and edge of F-CF obviously have a lot of pores when compared with CF, as shown in the magnified SEM image of Figs. 1(d) and 1(g). Therefore, we believe that the reaction between CFs and HF changed the surface morphology and the structure of the CFs greatly due to the strong acidity and corrosivity of HF and weakened the bonds between carbon atoms. The as-formed rough surface of F-CFs was subjected to ultrasonic exfoliation to obtain F-GQDs.

The transmittance electron microscopy (TEM) images (Fig. 2) clearly show the microstructure, morphology, and size distribution of as-prepared F-GQDs. The overall appearance of F-GQDs with uniform distribution is shown in

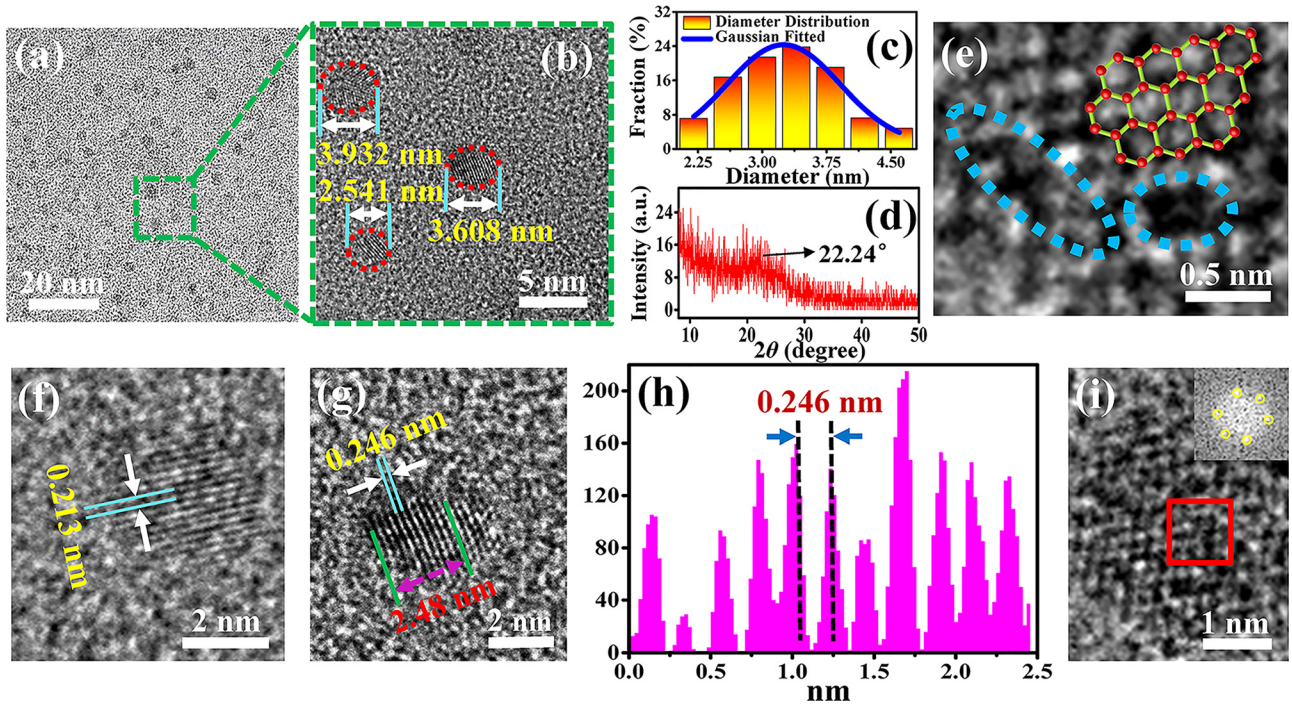

FIG. 2. Microstructure and morphology of as-prepared F-GQDs: (a) TEM image of F-GQDs. (b) Diameters of specific F-GQDs. (c) The diameter distribution of F-GQDs, the blue line is the Gaussian fitted curve. (d) XRD pattern of F-GQDs. (e)–(g), The HRTEM images of single F-GQD. (h) The line profile of the lattice finger is shown in (g). (i) FFT pattern (inset) of a selected area (red square).

Fig. 2(a), and the area highlighted in green is magnified in Fig. 2(b). The typical spherical F-GQDs within 5 nm in diameter could be observed in correspondence with the characteristics of GQDs proposed previously.[20]

Figure 2(c) shows the diameter distribution of F-GQDs in Fig. 2(a). The sizes of F-GQDs follow a Gaussian fitted distribution ranging from 2 nm to 5 nm with an average diameter of 3.25 nm, and the full width at half-maximum (FWHM) is 1.54 nm. The F-GQDs have a broadened diffraction peak centered at around $2\theta = 22.24°$ due to their small size, according to the x-ray diffraction (XRD) pattern shown in Fig. 2(d). The calculated d-spacing of F-GQDs is 0.399 nm by the Bragg equation, which is larger than graphite (0.335 nm) because the introduction of other functional groups has enlarged the interlayer.[21]

The arrangement of carbon atoms in F-GQDs is a hexagonal honeycomb structure with six carbon atoms packed around the center of a benzene ring, and crystal defects such as dislocations and vacancies (dashed area) are obvious, shown in Fig. 2(e). These defects are introduced by the processes of reaction with acid and surface corrosion. Figures 2(f) and 2(g) show the single F-GQD with special lattice fringes of $d = 0.213$ nm and 0.246 nm, which corresponds to $(\bar{1}\ 1\ 0)$, $(1\ \bar{1}\ 0)$ in-plane planes and $(1\ 0\ 0)$ basal plane of graphite, respectively.[1,20]

Figure 2(h) shows the line profile of the lattice fringes shown in Fig. 2(g), illustrating that the F-doping did not change the fundamental lattices of GQDs. The fast Fourier transform (FFT) pattern of the area highlighted in red is shown in the inset of Fig. 2(i). It exhibits the carbon hexagonal lattice structure that is the characteristic of graphene. From the above morphology characterizations, we can infer that F-doping did not change the crystal structure of GQDs but led to the lattice defects.

To investigate whether the doping with F was effective, the samples were characterized by Fourier transform infrared (FTIR) spectroscopy and Raman spectroscopy. The FTIR spectra of GQDs and F-GQDs are presented in Fig. 3(a). Compared with GQDs, there is a significant stretching of vibration absorption peak at 1030 cm^{-1} due to C-F bonds according to Sadtler Handbook of Infrared Spectra.[22] The absorption peak (1100 cm^{-1}) of the C-O band of F-GQDs is weaker than that of GQDs, which may be attributed to the incorporation of fluorine. The typical absorption peak of C=C bands was located at 1650 cm^{-1}. Figure 3(b) displays the Raman spectra of GQDs and F-GQDs. The D peak of F-GQDs exhibits a blue shift by 3 cm^{-1} in contrast to GQDs, indicating that fluorine can slightly soften the Raman scattering, and that peak is also getting wider and stronger. Both G peaks are centered at 1600 cm^{-1}. Furthermore, the calculated relative D-band to G-band intensity ratio (I_D/I_G) of F-GQDs is 1.12, larger than GQDs with 0.65, which indicates that the F-GQDs possess a higher disorder of arrangement regarding their crystalline structure.[23] This is consistent with the lattice defects as shown in Fig. 2(e), which is related to the increased sp^3 by introducing the C-F band.

To investigate the optical properties of F-GQDs, we studied the ultraviolet-visible (UV-Vis) absorption spectra, photoluminescence (PL) spectra, and photoluminescence excitation

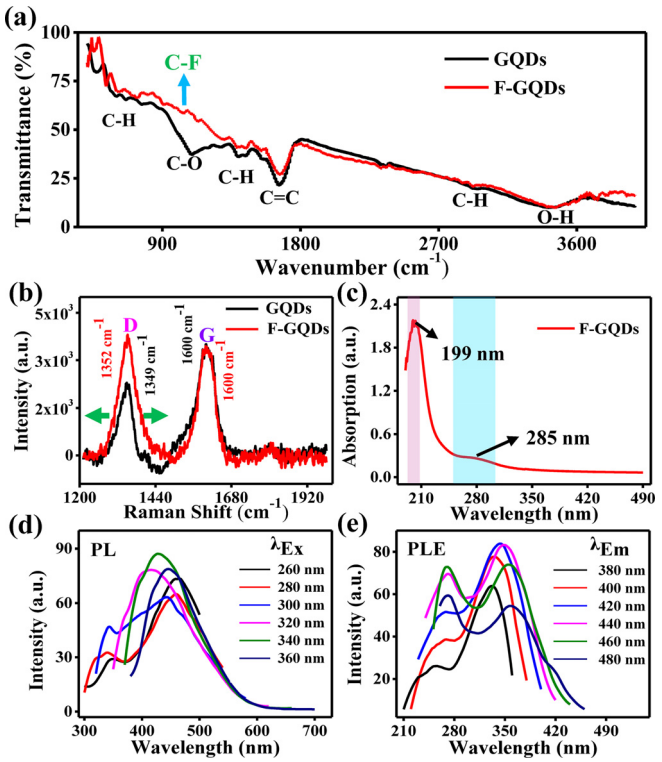

FIG. 3. (a) FTIR and (b) Raman spectra of F-GQDs/GQDs. (c) UV-Vis absorption spectra of F-GQDs aqueous solution. The (d) PL and (e) PLE spectra of aqueous F-GQD solution.

(PLE) spectra of aqueous F-GQDs solution. As shown in Fig. 3(c), there are two absorption peaks at 199 nm and 285 nm, which are similar to those of as-reported chlorine doped GQDs (Cl-GQDs).[24] The peak at 199 nm of F-GQDs exhibits a blue shift of 29 nm as compared with GQDs at 228 nm,[1] since the doping of fluorine effectively modulated the bandgap of GQDs.

A detailed PL study was carried out using different excitation wavelengths ranging from 260 nm to 360 nm, as shown in Fig. 3(d). Two PL peaks can be observed when λ_{Ex} is less than or equal to 300 nm, and the characteristic peak at shorter wavelength resulted from the $\sigma \rightarrow \sigma^*$ transitions of electrons,[20] which requires a higher energy than $\pi \rightarrow \pi^*$ transitions. The maximum PL intensity appeared at 428 nm under excitation at 340 nm, which has a red shift of 20 nm, indicating a lower excitation energy demand compared with the F-GQDs prepared by the other method.[18] Figure 3(e) shows the PLE spectra of as-prepared F-GQDs; two PLE peaks exist with different λ_{Em}, and their wavelength is less than relevant λ_{Em}, in accordance with the PL spectra, showing good UV fluorescence properties.

The process for preparing F-GQDs is illustrated in Fig. 4(a). The element composition and chemical bonds of a material are closely related to its method of preparation. To further explore the composition and chemical bonds of the F-GQDs, XPS was used for characterization. Figure 4(b) shows the full-scan XPS spectrum of F-GQDs with C 1s orbital at 284.8 eV, O 1s at 532 eV, N 1s at 400 eV (from the residual NMP), and F 2s at 25.6 eV, which confirmed the existence of fluorine.

In XPS spectra of O 1s (Fig. 4(c)), the oxygen-related chemical bonds are located at 530.6 eV, 531.4 eV, 532.1 eV,

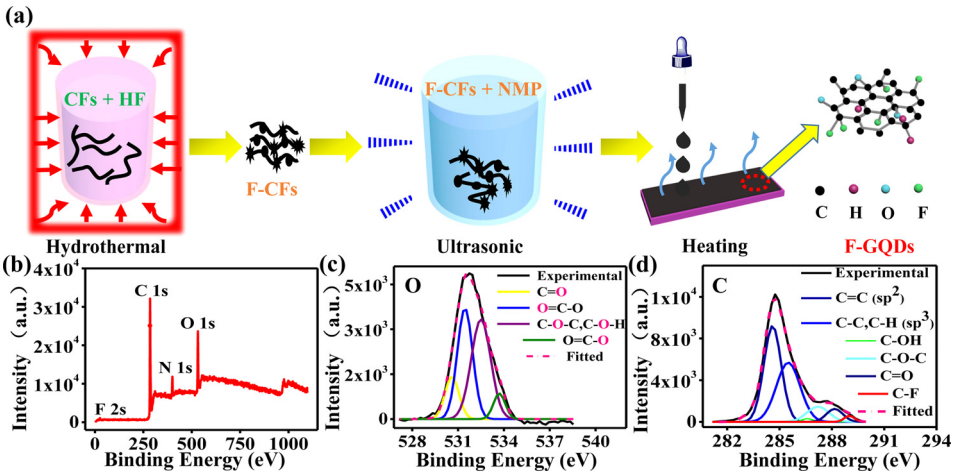

FIG. 4. (a) The schematic illustration of the preparation of F-GQDs. (b) The full-scan XPS spectrum of F-GQDs. (c) The O 1s XPS spectrum. (d) The C 1s XPS spectrum.

and 533.7 eV. In Fig. 4(d), the XPS spectra of C 1s can be deconvoluted into six peaks centered at around 284.5 eV (sp^2), 285.4 eV (sp^3), 283.5 eV (C-OH), 287.1 eV (C-O-C), 288.1 eV (C = O), and 288.9 eV (C-F).[25] By XPS analysis, it can be concluded that C-F covalent bonds exist in the F-GQDs, which well modified the surface structure and transformed the properties of GQDs.[26]

Due to the excellent UV absorption of as-prepared F-GQDs, we fabricated a vertical UV photodetector based on F-GQDs to explore the applications in optoelectronic fields. The diagram for fabrication of the UV detector based on F-GQDs is shown in Fig. 5(a). Indium tin oxide (ITO) with glass substrates (2.5 × 2.5 cm) was chosen as the transparent electrode, then a thin layer of poly(3,4-ethylenedioxythiophene):poly (styrenesulfonate) (PEDOT:PSS) (Sigma-Aldrich) was spin-coated onto ITO as the hole transport layer. The PEDOT:PSS dried out at 80 °C for 15 min. Then, the PEDOT:PSS layer was spin-coated with a liquid mixture of F-GQDs and PEDOT:PSS ($m_{\text{F-GQDs}}$: $m_{\text{PEDOT:PSS}}$ = 1:19). After the same drying process, aluminum electrodes were deposited on top by thermal evaporation. The vertical structure of the F-GQDs hybrid UV detector is shown in Fig. 5(b) with the F-GQDs acting as light sensitive and photoelectron absorbing layer.

The J–V curve of the UV detector irradiated by $\lambda = 365$ nm light under the conditions of 0 mW·cm^{-2}, 0.16 mW·cm^{-2}, and 0.47 mW·cm^{-2} is shown in Fig. 5(c). The current densities have improved a lot under irradiation, increased together with the photo power density, showing that the device has good photoelectric properties. In the log(J)–V curve shown in Fig. 5(d), the unoptimized device had an exceptionally big ratio of photocurrent to dark current of magnitude $\sim 10^5$, indicating a promising application in UV detection.

We discussed the responsivity (R) and detectivity (D^*) of the photodetector, expressed by Eqs. (1) and (2)[27]

$$R = J_{ph}/P_{opt}, \tag{1}$$

$$D^* = \frac{R}{\sqrt{2q/J_d}}, \tag{2}$$

where J_{ph} is the photocurrent density, P_{opt} is the photo power density, q is the absolute electron charge (1.6×10^{-19} coulombs), and J_{d} is the dark current density.

The value of R is little small in Fig. 5(e), but it increased together with the increase in the reverse bias voltage, and the D^* could stabilize at around 10^{12} Jones (1 Jones = 1 cm·Hz$^{1/2}$·W^{-1}).

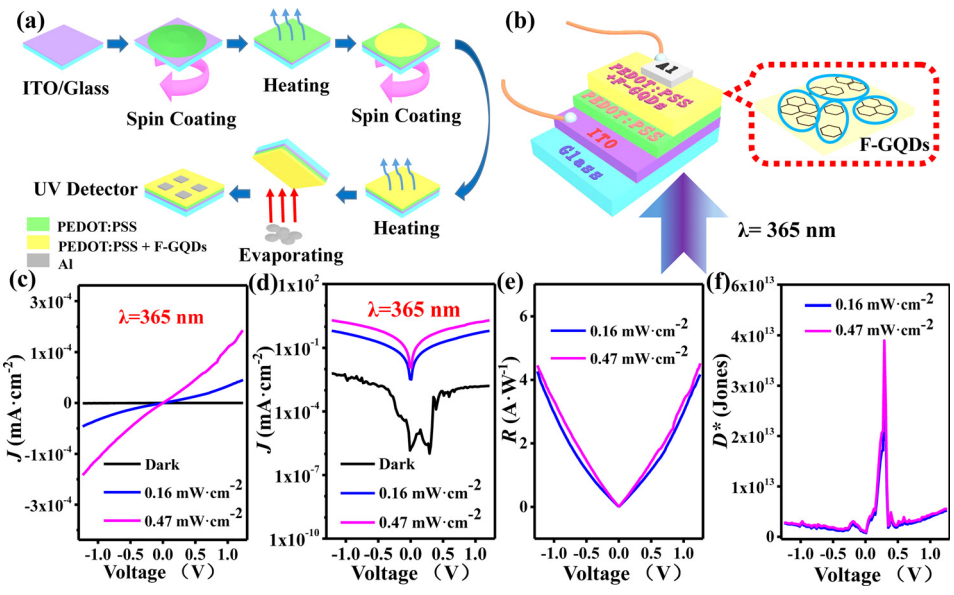

FIG. 5. (a) The schematic illustration for fabrication of the F-GQDs hybrid UV detector. (b) The schematic diagram of the F-GQDs hybrid UV detector. The device performance of the F-GQDs hybrid UV detector: (c) J-V curves. (d) log(J)-V curves. (e) R (Responsivity)-V curves. (f) D^* (Detectivity)-V curves.

TABLE I. The ideality factors (η) and barrier heights (Φ_b) of the F-GQDs hybrid UV detector under different power densities.

Power density (mW·cm^{-2})	H	Φ_b (eV)
Dark	0.88	1.25
0.16	0.69	0.73
0.47	0.69	0.70

To study the underlying physical mechanism, we applied thermionic emission theory[28] to research the electric transportation within the UV detector based on F-GQDs

$$J = J_o\left[\exp\left(\frac{qv}{\eta k_B T}\right) - 1\right], \tag{3}$$

where J_0 is the reverse saturation current density, V is the bias voltage, η is the ideality factor, k_B is the Boltzmann constant, and T is the absolute temperature. As for Equation (3), since $qV \gg \eta k_B T$, thus, $\ln(J) = \ln(J_0) + \frac{qv}{\eta k_B T}$, $\eta = (\frac{d\ln J}{dv}\frac{k_B T}{q})^{-1}$ therefore, the ideality factor η can be calculated from the slope of the $\ln(J)$–V curve.

Barrier heights Φ_b can be calculated using the Richardson equation

$$J_0 = A^* T^2 \exp\left(-\frac{q\varphi_b}{k_B T}\right), \tag{4}$$

where $A^* = \frac{4\pi q m^* {k_B}^2}{h^3}$ is the effective Richardson constant, and m^* is the effective electron mass, which could be calculated by

$$m^* = m^*(\text{F-GQDs})\omega(\text{F-GQDs}) + m^*(\text{PEDOT:PSS})\omega(\text{PEDOT:PSS}), \tag{5}$$

where m^* (F-GQDs) ≈ 0.05,[24] m^* (PEDOT:PSS) ≈ 0.28.[29]

The ideality factor (η) and barrier heights (Φ_b) of the UV detector based on F-GQDs are calculated using the above equations and are listed in Table I. One can find that η is close to 1, indicating that the device had a good rectification effect and is expected to be applied in the field of high-performance photodetectors. The unoptimized device maintained an undegraded performance after a long-term (for 8 months) storage, which means F-GQDs possess excellent stability.

In conclusion, we used the degreasing cotton as the carbon source and annealed it at 1000 °C for 1 h to prepare CFs. After that, the reaction precursor F-CFs were obtained by hydrothermal reaction between CFs and HF. Finally, through ultrasonic liquid phase exfoliation, we prepared F-GQDs. Herein, we discussed the fluorination mechanism of CFs in detail, which is attributed to the corrosion by HF. The doping of fluorine atoms can roughen the surface of CFs and facilitate the exfoliation to obtain F-GQDs. Through FTIR and XPS characterization, it was confirmed that F was incorporated into GQDs, and the covalent bonds were created. We invented a facile, simple, handy synthesis route to prepare F-GQDs, and the as-prepared F-GQDs showed good UV absorption. The unoptimized device based on F-GQDs was achieved with a ratio of photocurrent to dark current of magnitude $\sim 10^5$, and its detectivity (D^*) could stabilize at around 10^{12} Jones at room temperature under $\lambda = 365$ nm light irradiation and reverse bias voltage. The long-term performance of the device remains undegraded after the storage for 8 months, which indicates that F-GQDs are a promising material for UV photodetectors.

This work was supported by National Natural Science Foundation of China (Grant Nos. 61106098, 51201150, and 11374250) and the Key Project of Applied Basic Research of Yunnan Province, China (Grant No. 2012FA003).

[1]L. B. Tang, R. B. Ji, X. K. Cao, J. Y. Lin, H. X. Jiang, X. M. Li, K. S. Teng, C. M. Luk, S. J. Zeng, J. H. Hao, and S. P. Lau, ACS Nano **6**, 5102 (2012).
[2]X. T. Zheng, A. Ananthanarayanan, K. Q. Luo, and P. Chen, Small **11**, 1620 (2015).
[3]Z. C. Huang, Y. T. Shen, Y. Li, W. J. Zheng, Y. J. Xue, C. Q. Qin, B. Zhang, J. X. Hao, and W. Feng, Nanoscale **6**, 13043 (2014).
[4]W. L. Ma and S. S. Li, Appl. Phys. Lett. **100**, 163109 (2012).
[5]J. Shen, Y. H. Zhu, X. l. Yang, J. Zong, J. M. Zhang, and C. Z. Li, New J. Chem. **36**, 97 (2012).
[6]M. L. Tsai, W. R. Wei, L. B. Tang, H. C. Chang, S. H. Tai, P. K. Yang, S. P. Lau, L. J. Chen, and J. H. He, ACS Nano **10**, 815 (2016).
[7]Q. Zhang, J. S. Jie, S. l. Diao, Z. B. Shao, Q. Zhang, L. Wang, W. Deng, W. D. Hu, H. Xia, X. D. Yuan, and S. T. Lee, ACS Nano **9**, 1561 (2015).
[8]S. J. Zhu, J. H. Zhang, C. Y. Qiao, S. J. Tang, Y. F. Li, W. J. Yuan, B. Li, L. Tian, F. Liu, R. Hu, H. N. Gao, H. T. Wei, H. Zhang, H. C. Sun, and B. Yang, Chem. Commun. **47**, 6858 (2011).
[9]C. M. Luk, L. B. Tang, W. F. Zhang, S. F. Yu, K. S. Teng, and S. P. Lau, J. Mater. Chem. **22**, 22378 (2012).
[10]Y. Li, Y. Zhao, H. H. Cheng, Y. Hu, G. Q. Shi, L. M. Dai, and L. T. Qu, J. Am. Chem. Soc. **134**, 15 (2012).
[11]L. B. Tang, R. B. Ji, X. M. Li, K. S. Teng, and S. P. Lau, J. Mater. Chem. C **1**, 4908 (2013).
[12]S. Kundu, R. M. Yadav, T. N. Narayanan, M. V. Shelke, R. Vajtai, P. M. Ajayan, and V. K. Pillai, Nanoscale **7**, 11515 (2015).
[13]R. R. Nair, W. Ren, R. Jalil, I. Riaz, V. G. Kravets, L. Britnell, P. Blake, F. Schedin, A. S. Mayorov, S. Yuan, M. I. Katsnelson, H. M. Cheng, W. Strupinski, L. G. Bulusheva, A. V. Okotrub, I. V. Grigorieva, A. N. Grigorenko, K. S. Novoselov, and A. K. Geim, Small **6**, 2877 (2010).
[14]D. K. Samarakoon, Z. F. Chen, C. Nicolas, and X. Q. Wang, Small **7**, 965 (2011).
[15]K. Tahara, T. Iwasaki, S. Furuyama, A. Matsutani, and M. Hatano, Appl. Phys. Lett. **103**, 143106 (2013).
[16]N. Liaros, A. B. Bourlinos, R. Zboril, and S. Couris, Opt. Express **21**, 21027 (2013).
[17]Y. Liu, Q. Feng, Q. H. Xu, M. Li, N. J. Tang, and Y. W. Du, Carbon **61**, 436 (2013).
[18]Q. Feng, Q. Q. Cao, M. Li, F. C. Liu, N. J. Tang, and Y. W. Du, Appl. Phys. Lett. **102**, 013111 (2013).
[19]Y. J. Shao, H. J. Yue, R. M. Qiao, J. Q. Hu, G. M. Zhong, S. Q. Wu, M. J. McDonald, Z. L. Gong, Z. Z. Zhu, W. L. Yang, and Y. Yang, Chem. Mater. **28**, 1026 (2016).
[20]L. B. Tang, R. B. Ji, X. M. Li, K. S. Teng, and S. P. Lau, Part. Part. Syst. Charact. **30**, 523 (2013).
[21]J. Peng, W. Gao, B. K. Gupta, Z. Liu, R. R. Abur knowledge, L. H. Ge, L. Song, L. B. Alemany, X. B. Zhan, G. H. Gao, S. A. Vithayathil, B. A. Kaipparettu, A. A. Marti, T. Hayashi, J. J. Zhu, and P. M. Ajayan, Nano Lett. **12**, 844 (2012).
[22]W. H. S. Sadtler, *The Sadtler Handbook of Infrared Spectra* (Bio-Rad Laboratories, Inc., Informatics Division, 1978).
[23]Y. Li, Y. Hu, Y. Zhao, G. Q. Shi, L. E. Deng, Y. B. Hou, and L. T. Qu, Adv. Mater. **23**, 776 (2011).
[24]J. H. Zhao, L. B. Tang, J. Z. Xiang, R. B. Ji, J. Yuan, J. Zhao, R. Y. Yu, Y. J. Tai, and L. Y. Song, Appl. Phys. Lett. **105**, 111116 (2014).
[25]J. M. Lee, S. J. Kim, J. W. Kim, P. H. Kang, Y. C. Nho, and Y. S. Lee, J. Ind. Eng. Chem. **15**, 66 (2009).
[26]J. T. Robinson, J. S. Burgess, C. E. Junkermeier, S. C. Badescu, T. L. Reinecke, F. K. Perkins, M. K. Zalalutdniov, J. W. Baldwin, J. C. Culbertson, P. E. Sheehan, and E. S. Snow, Nano Lett. **10**, 3001 (2010).
[27]X. Gong, M. H. Tong, Y. J. Xia, W. Z. Cai, J. S. Moon, Y. Cao, G. Yu, C. L. Shieh, B. Nilsson, and A. J. Heeger, Science **325**, 1665 (2009).
[28]S. Tongay, M. Lemaitre, X. Miao, B. Gila, B. R. Appleton, and A. F. Hebard, Phys. Rev. X **2**, 011002 (2012).
[29]H. B. Akkerman, R. C. G. Naber, B. Jongbloed, P. A. van Hal, P. W. M. Blom, D. M. de Leeuw, and B. de Boer, Proc. Natl. Acad. Sci. U.S.A. **104**, 11161 (2007).